HHS Public Access

Author manuscript

Neuroimage. Author manuscript; available in PMC 2016 May 01.

Published in final edited form as:

Neuroimage. 2015 May 1; 111: 513–525. doi:10.1016/j.neuroimage.2015.01.023.

Pre-stimulus functional networks modulate task performance in time-pressured evidence gathering and decision-making

Jason Samuel Sherwin[a,b,*,1], **Jordan Muraskin**[a,1], and **Paul Sajda**[b]

Jason Samuel Sherwin: jason.sherwin@downstate.edu; Jordan Muraskin: jsm2112@columbia.edu; Paul Sajda: psajda@columbia.edu

[a]Department of Biomedical Engineering, Columbia University, New York, NY 10027, USA

[b]Human Research and Engineering Directorate, U.S. Army Research Laboratory, Aberdeen Proving Ground, MD 21005, USA

Abstract

Rapid perceptual decision-making is believed to depend upon efficient allocation of neural resources to the processing of transient stimuli within task-relevant contexts. Given decision-making under severe time pressure, it is reasonable to posit that the brain configures itself, prior to processing stimulus information, in a way that depends upon prior beliefs and/or anticipation. However, relatively little is known about such configuration processes, how they might be manifested in the human brain, or ultimately how they mediate task performance. Here we show that network configuration, defined *via* pre-stimulus functional connectivity measures estimated from functional magnetic resonance imaging (fMRI) data, is predictive of performance in a time-pressured Go/No-Go task. Specifically, using connectivity measures to summarize network properties, we show that pre-stimulus brain state can be used to discriminate behaviorally correct and incorrect trials, as well as behaviorally correct commission and omission trial categories. More broadly, our results show that pre-stimulus functional configurations of cortical and sub-cortical networks can be a major determiner of task performance.

Keywords

Baseball; Decision-making; Functional magnetic resonance imaging; Functional connectivity; Graph-based networks; Machine learning

Introduction

Pre-stimulus brain state, measured at a variety of spatial and temporal scales, has been shown to modulate upcoming task performance. For instance, studies in humans using electroencephalography (EEG) and magnetoencephalography (MEG) have shown that the power and/or phase of pre-stimulus alpha oscillations is correlated with performance (Hanslmayr et al., 2007; Linkenkaer-Hansen et al., 2004; Thut et al., 2006; Zhang et al.,

*Corresponding author at: Martinez-Conde Laboratory Department of Ophthalmology SUNY Downstate Medical Center 450 Clarkson Avenue, MSC 58 Brooklyn, NY 11203-2012, USA. Tel: +1 (718) 221-5389.

[1]Tel.: +1 708 373 7943.

2008). EEG and MEG, however are inherently limited by low spatial resolution. Their use for estimating current sources and scalp-level pre-stimulus modulators are biased toward the strongest cortical sources and typically ignore the interaction between these and weaker sources, as well as those that may be sub-cortical. Alternatively, the blood oxygen level dependent (BOLD) signal from functional magnetic resonance imaging (fMRI) provides whole-brain imaging that in theory provides a functional measurement of pre-stimulus brain state, albeit at a coarser temporal resolution. Most studies investigating pre-stimulus fMRI have largely limited their analyses to isolated regions of interest (ROIs) known *a priori* to be relevant for a given task (Hesselmann et al., 2008; Hsieh et al., 2012; Park and Rugg, 2010; Shibata et al., 2008).

Recently, functional connectivity analysis of BOLD signals during resting state and stimulus presentation has shown that distributed networks of neural substrates are engaged in both idle and active modes of attention (Hasson et al., 2012; Honey et al., 2007, 2009; McIntosh, 1999; McIntosh et al., 1997). For visually driven perceptual decision-making it has been shown that distributed neural substrates affect task difficulty and early visual perception (Hartstra et al., 2010; Philiastides and Sajda, 2007; Simmonds et al., 2008). However, characterization of the relationship between these substrates and how interactions between them may impact task performance has been lacking.

Here we used whole-brain imaging and graph-based network analysis to investigate the role of pre-stimulus brain state on task performance. Our rationale for this approach is that such a network characterization of task-relevant neural substrates would capture distributed BOLD activity across the entire brain. Graph theoretic approaches have been shown to be useful constructs for characterizing brain state, where changes in state are reflected in network parameters and configuration (Bressler and Menon, 2010; Bullmore and Sporns, 2009; Sporns, 2011). Features of the graph that can be measured and reflect graph/network configuration include, for example, the k-core decomposition which measures network properties related to node centrality and connectedness (Alvarez-Hamelin et al., 2008). Another commonly used graph measure to assess configuration is the random edge attack (REA), where selected structures of the network are systematically removed (Achard et al., 2006; Albert and Barabasi, 2002; van den Heuvel and Sporns, 2011).

The specific graph theoretic approach we use is based on the work of Ekman et al. (2012). Specifically, Ekman et al. used a graph-based network analysis to study task related network configurations in motion/color perceptual decision making. While novel in its techniques and experimental design, this study utilized stimuli known to activate particular ROIs (*e.g.*, V4 for color perception and MT for motion perception). These ROIs were found with a task-driven algorithm, so the computationally expensive and exploratory step of calculating pairwise connectivity between all fMRI voxels (>~20,000 in standard MNI space) was not required. While the *a priori* functional information did not guide their algorithm, it provided a useful check on its veracity. Their graph-based approach further separated pre-stimulus networks into core and periphery sub-networks, showing that such distinctions could be used to isolate task-specific regions (*e.g.*, V4 and MT) and task-general brain regions (*e.g.*, frontal cortices), whose functional properties could be differentiated using standard graph theory measures, such as degree, efficiency and betweenness centrality. Such analyses build on the

'rich-club' concept that brain networks are functionally mediated by densely connected central hubs (van den Heuvel and Sporns, 2011).

The work we present here uses this graph-based approach to investigate the role of pre-stimulus network configuration on task performance given a rapid evidence accumulation decision-making (READ-M) paradigm. The READ-M paradigm requires subjects to employ visual memory, motion assessment, and a rapid behavioral response or inhibition of response, all while under time pressure. We refer to this as 'the baseball paradigm' as it requires the subject to judge whether a simulated trajectory of a circular object matches or does not match a pre-stimulus trajectory cue. As in the game of baseball, the subject – or 'hitter' – must rapidly decide his/her course of action (or inhibition of action) given a fast-moving visual stimulus. This entire process typically must take place in less than half a second. Previous studies have shown that this paradigm engages anatomically separated neural substrates during stimulus perception and subsequent decision formation (Ekman et al., 2012; Sherwin et al., 2012). This paradigm also falls into the general class of Go/No-Go tasks, which have been shown to involve local and distant brain regions, such as the inhibition network for No-Go and an execution network for Go decisions (Simmonds et al., 2008). Our hypothesis is that the pre-stimulus configuration of brain networks, represented *via* these graphical constructs, switch configuration based on the subject's anticipation of the trajectory cue and that this switch subsequently predicts task performance.

Materials and methods

Subjects

Eleven subjects participated in the study (all male, mean age = 21.6 years, range = 18–30 years). None of the subjects had professional or collegiate baseball experience. All subjects reported normal or corrected vision and no history of neurological problems. Informed consent was obtained from all participants in accordance with the guidelines and approval of the Columbia University Institutional Review Board.

Stimuli overview

For the visual stimulus, subjects viewed 5 blocks of 90 simulated baseball pitches (see pitch simulations below) on a computer monitor with a mean jittered inter-stimulus interval (ISI) of mean = 3000 ms, SE = 225 ms. The ISI and stimulus presentation was optimized using *optseq2* program (Dale, 1999). This program is a tool for automatically scheduling events for rapid-presentation event-related fMRI experiments and it jitters the events such that the overlap in estimated hemodynamic response is removed. Subjects viewed the paradigm through VisuaStim Digital System (Resonance Technology) 600 × 800 goggle display. The simulated view was that of where the catcher would sit on a standard baseball diamond, *i.e.*, at the end point of the pitch trajectory (horizontal view 3.93°, vertical view 1.12°).

Pitch simulations

Each simulated pitch was identified only by its trajectory, although in real-life baseball hitting the pitch is identifiable by other features, such as spin. Henceforth, we refer to 'pitch' and 'trajectory' synonymously. This trajectory moved within the plane of the screen and

simulated movement in the direction perpendicular to this plane. For each frame of the simulated pitch, an isoluminant green circle was plotted on a gray background. The size of the circle increased as it approached the viewer, so as to give the illusion of depth. When the ball crossed 'home plate,' the circle disappeared.

As in previous work (Muraskin et al., 2013; Sherwin et al., 2012) using a related paradigm, each pitch was created in three dimensions of space using a differential equation solver in Matlab 2010a (Mathworks, Natick, MA, USA) (see pitch simulations below) and presented *via* PsychToolbox (Brainard, 1997; Pelli, 1997).

Most baseball pitches can be simulated using 6-coupled differential equations (Adair, 1995; Armenti, 1992) and we used these equations to simulate each pitch.

Equations of motion for simulated pitch trajectories:

$$\frac{dx}{dt}=v_x \quad (1)$$

$$\frac{dy}{dt}=v_y \quad (2)$$

$$\frac{dy}{dt}=v_z \quad (3)$$

$$\frac{dv_x}{dt}=-F(v)vv_x+B\omega\left(v_z\sin\phi-v_y\cos\phi\right) \quad (4)$$

$$\frac{dv_y}{dt}=-F(v)vv_y+B\omega v_x\cos\phi \quad (5)$$

$$\frac{dv_z}{dt}=-g-F(v)vv_z-B\omega v_x\sin\phi \quad (6)$$

$$F(v)=0.0039+\frac{0.0058}{1+e^{(v-v_d)/\Delta}}. \quad (7)$$

The first three equations specify the change in spatial location in each direction, which equals the velocity of the baseball. The last four equations specify the accelerations due to the drag ($F(v)$), the Magnus force (B), and gravity (g) acting on the baseball. After specifying the initial conditions (x_0, y_0, z_0, v_{x0}, v_{y0}, v_{z0}, ω (rotational frequency)), the 6 ordinary differential equations were solved in MATLAB.

We simulated three different pitch categories with these equations. The three pitch categories – fastball, curveball, and slider – have well-defined individual initial conditions. To create each pitch category, we varied the initial velocity and the rotation angle. We also

varied pitches within each category so that no two pitches from the same category followed the exact same trajectory. To this end, the initial conditions of the trajectory were also jittered within each pitch category.

Behavioral paradigm

Subjects were presented with a pitch chosen at pseudorandom from the three pitch categories (here, 'fastballs', 'curveballs' and 'sliders'). Preceding the pitch, a horizontal bar (horizontal extent 3.93°, vertical extent 0.28°) appeared onscreen for a mean time of 819 ms, SD = 3.1 ms, during which time the horizontal length of the bar shrunk at a constant rate until it disappeared. For pitches coming from a right-handed pitcher, the horizontal bar shrank in size to the left; *vice versa* for pitches from a left-handed pitcher. Once the bar shrank completely in length, the pitch began from this point on the screen. While the horizontal bar was onscreen, a single-letter cue indicated the possible pitch category to follow ('F' for fastball, 'C' for curveball, or 'S' for slider; horizontal view 0.28°, vertical view 0.28°). The subject was instructed to execute a Go/No-Go task in relation to these stimuli.

A subject executed a keyboard button response only if the pitch category cue matched the actual pitch category. For instance, if the cue above the horizontal bar was an 'F' and a fastball was to follow then the subject would be expected to execute a button response (*i.e.*, a 'Go'). However, if a curveball or slider trajectory was to follow the same cue then the subject would be expected to restrain from executing a button response (*i.e.*, a 'No-Go'). Subjects were told to respond while the ball was still on the screen. For correct 'Go' and 'No-Go' decisions, the subject received visual feedback after the pitch's completion in the form of a cross ('+'). For incorrect 'Go' and 'No-Go' decisions, the subject received visual feedback in the form of a dash ('−'). A 'Go' response was not considered correct unless the category of pitch cue matched the category of pitch stimulus *and* the button response occurred before the pitch's end.

We further grouped all decisions into behaviorally 'Correct' and 'Incorrect' trial categories. Correct trial categories included both Correct Go and Correct No-Go decisions, while Incorrect trial categories included the remainder, *i.e.*, Incorrect Go, Incorrect No-Go and late Go responses.

All button responses were executed with the right hand index finger, regardless of handedness. In an initial practice phase, we trained subjects until they scored an accuracy of at least 60% (chance accuracy ~50%). This training criterion insured performance above chance at the task. Once this criterion was met, the 5 blocks began and fMRI data were recorded.

Data acquisition

Data acquisition was performed using a 3 T Philips Achieva MRI scanner (Philips Medical Systems) equipped with an 8-channel SENSE head coil. Functional echo-planar image (EPI) data was collected with isotropic 3 mm voxel sizes. We covered the entire brain by obtaining 35 slices of 64 × 64 voxels using a 2000 ms repetition time and 20 ms echo time.

We also acquired a single-volume high-resolution (2 × 2 × 2 mm) EPI image and a 1 × 1 × 1 mm T1-weighted MPRAGE for each subject for registration. Respiration and heart rate measures were recorded for all subjects using the scanner's respiratory bellows monitor and pulse oximeter (Philips Healthcare, Best, The Netherlands) and continuously sampled at 500 Hz throughout each scan.

fMRI post-stimulus BOLD and searchlight analyses

Using FSL (FMRIB Software Library; Smith et al., 2004), we performed slice-timing correction, motion correction, and 0.01 Hz high-pass filtering on the functional data. We did not apply any spatial smoothing filters as advised for searchlight analyses (Kriegeskorte et al., 2006). Functional and structural images were registered to a standard Montreal Neurological Institute (MNI) brain template after brain extraction, and each subject's image registration was checked manually to ensure proper alignment. Data were then subsampled to 4 mm resolution isotropic.

We utilized a general linear model (GLM) to determine parameter estimates, or PEs (β), for each trial category in each subject's voxel-space (Fig. 1A). Post-stimulus time periods are indicated by non-zero heights to regressors, including the one for response time variability when a motor response was present. For Incorrect trial categories, only incorrect No-Go decisions were used because there were significantly fewer incorrect Go decisions (two-sided paired *t*-test, $t(10) = 5.29$, $p < 10^{-3}$; Go: mean = 39, SE = 4; No-Go: mean = 83, SE = 8). After regressing out the motion and physiological noise from cardiac and respiratory pulsations (PhLEM toolbox, RETROICOR), we created regressors for behaviorally correct and incorrect trial categories using box-car functions whose height was non-zero only when the pitch was onscreen. Response regressors were modeled as a variable height box-car function proportional to response time. We did this for each of the five (5) blocks of each of the eleven (11) subjects, *i.e.*, we ran a Level 1 GLM analysis.

We registered all subjects to MNI standard space and then performed a searchlight analysis to analyze BOLD response by trial category. We did this only for gray matter voxels, segmented using FSL. We segmented gray and white matter with 5 mm full width half maximum (FWHM) smoothing for each subject, registered all subjects to MNI standard space, and then averaged across subjects, so that a voxel was considered gray matter if it contained at least 20% gray matter. We then identified ROIs that discriminated trial category using regularized logistic regression (Conroy and Sajda, 2012) (illustration of hyperplane solution shown in Fig. 1B). Specifically, we constructed an 8 mm-radius sphere around each gray-matter voxel, within which the PEs of behaviorally correct trial categories were maximally discriminating from those of behaviorally incorrect trial categories. It is important to note that behaviorally correct trial categories includes Correct Go (motor response present) and Correct No-Go (motor response absent) trial categories, while behaviorally incorrect trial categories include Incorrect No-Go (motor response present) trial categories; thus the discrimination is between behavioral performance outcomes, rather than the presence/absence of a motor response. When leaving one subject out for testing purposes, we removed all five blocks of behaviorally correct and incorrect trial category PEs. In this way, we cross-validated our classifier across all subjects.

Having done the searchlight analysis at each gray-matter voxel, we generated an area under the ROC (AUC) map (left half of Fig. 2A) that we transformed into a p-value map. We determined significance using a permutation testing using a Monte Carlo randomization procedure (Bjornsdotter et al., 2011). Specifically, we calculated 1000 permutations to establish a statistical threshold AUC and resulting p-value at each voxel ($1 - p_{adj}$, where p_{adj} is the FDR-adjusted p-value, is shown in the right half of Fig. 2A). All p-values were adjusted with the false discovery rate (FDR) method (Benjamini, 1995).

Brain parcellation and pre-stimulus network construction

We parcellated the brain into 12 mm non-overlapping nodes centered on the lowest p-value (*i.e.*, most significant) voxels. The algorithm, illustrated in Fig. 2B, proceeded as follows: the lowest p-value voxel was found and circumscribed by a 12 mm sphere, after which all voxels falling within this sphere are removed from further consideration and included within node 1; the next lowest p-value voxel was then found and circumscribed by another 12 mm sphere, only if this new sphere did not intersect with the previous one, after which all voxels falling within this sphere are removed from further consideration and included within node 2; the procedure continues until there is no more room in the standard space brain for another non-overlapping 12 mm sphere or the last significant p-value has been found. This procedure yielded 57 sphere-nodes in the MNI space each with $p < 0.05$, FDR-corrected.

Having defined the nodes of our network, we determined the edges from pre-stimulus functional data. We did so by using each subject's connectivity matrix of the sub-category of each trial category (*e.g.*, Incorrect No-Go being the connectivity matrix for the Incorrect trial category; Correct Go and Correct No-Go being those for the Correct trial category). Illustrated in the left half of Fig. 2C, for each trial category, we extracted and concatenated mean pre-stimulus global-mean-removed functional data within each node. Here, pre-stimulus was defined to be any time between the feedback of the previous trial (*i.e.*, a visual feedback of '+' or '−') and the TR before the start of the pitch of the upcoming trial. These time points are indicated in bold frames in Fig. 1 and Fig. 2. We accounted for the hemodynamic lag by assuming a mean 5-s delay from stimulus timing. From the *optseq2* stimulus presentation, we had a 3000 ± 225 ms ISI, and with a TR of 2 s, each trial yielded approximately two data points, though some yielded more and some less. We did not include the small percentage of trials that had ISIs less than 2 s, only using data from at least 1TR (*i.e.*, 2 s) before the start of the pitch trajectory. We then up-sampled by a factor of 4 to transform the 0.5 Hz functional signal to 2 Hz. Previous connectivity analyses have shown that up-sampling can aid in connectivity analysis (McFarlin et al., 2013). Following other functional connectivity analyses (Achard et al., 2006), we bandpass filtered the functional signal to 0.06–0.12 Hz.

We calculated a thresholded connectivity matrix for each subject and trial category *via* the correlation coefficient of each pair of nodes. The thresholding was the result of a non-parametric permutation test that established a $p = 0.05$ FDR-corrected value for correlation coefficient in all elements of the matrix. Having upsampled the BOLD signal to 2 Hz, this permutation test insured that we would not artificially inflate the p-values determined from a parametric approximation of Pearson correlation p-value. The permutation specifically was

applied to the time points of the jth node and then the correlation coefficient to the ith node was recalculated, $i \neq j$. Although negative correlations also passed FDR correction ($p < 0.05$), only positive correlations that passed FDR correction were used for further analysis, as done in previous work (Achard et al., 2006; Ekman et al., 2012). Consequently, negative correlations and positive correlations whose p-values fell below the FDR threshold were set to zero. The networks were then constructed from these thresholded connectivity matrices. We illustrate these networks in the right half of Fig. 2C, where each node's location is organized according to the energy minimization of Kamada and Kawai (1989).

Network feature calculation

We next calculated graph-theoretic measures to summarize the properties of each of these 57-node networks (illustrated in Fig. 2D). A summary of these measures is shown in the Supplementary data as Table S1. Local measures have values at each node in the network, while global measures apply to the entire network. Three key measures used are degree, efficiency and betweenness centrality, all of which are calculated from the weights (specifically, thresholded Pearson correlation coefficient) connecting a given node to others in the network. Briefly, local degree (k) is defined as the sum of all weights connecting a given node to all others. Local efficiency (E) is defined as the sum of the distances between a given node to all others, normalized by a factor dependent on the number of nodes in the network. Finally, betweenness centrality (BC) is a measure of the density of shortest paths passing through a given node. Precise definitions of these measures and all others used can be found elsewhere (Rubinov and Sporns, 2010), but they were chosen based on their use in an earlier study on decision-making performance (Ekman et al., 2012) and other studies on functional connectivity (Achard et al., 2006; Bullmore and Sporns, 2009). For network measures depending on distance, we applied an inverse transformation to the thresholded correlation coefficient as used in these previous studies. We calculated these network measures for whole networks (upper half of Fig. 2D), core sub-networks and periphery subnetworks (lower half of Fig. 2D). We utilized the Brain Connectivity Tool-box to calculate these measures (Rubinov and Sporns, 2010).

Network feature analysis: random edge attack response variation by trial category

We analyzed network features by trial category using a standard method of network analysis and a new approach in which elastic net regularized logistic regression is used as a machine learning approach.

For the standard analysis, we performed a random edge attack (Achard et al., 2006; Albert and Barabasi, 2002; van den Heuvel and Sporns, 2011), which is defined for weighted networks. A random edge attack (REA) analysis consists of multiple simulations in which a sequential number of edges are removed from the network before recalculating global network measures. We created networks for each trial category by meaning all subjects' thresholded connectivity matrices within that category, thus creating a network for each (N_{CG}, N_{CNG}, N_{ING}). We then pseudo-randomly removed up to five (5) edges sequentially from each network and assessed the impact on particular global features of the whole network. Since this analysis can be done for any network, we applied the same procedure to core and periphery sub-networks of each trial category too (C_{CG}, C_{CNG}, C_{ING}; P_{CG}, P_{CNG},

P_{ING}). Before doing so, we isolated core and periphery sub-networks using the k-core decomposition method, a recursive pruning technique applied before to functional imaging data (Carmi et al., 2007; Ekman et al., 2012). Though it is more usually defined for any unweighted network, we used an adaption of the algorithm for a weighted network (Garas et al., 2012). Briefly, the k-core algorithm finds the largest subnetwork comprising nodes of degree k by recursively removing nodes with degree lower than k until no nodes remain. Once this subnetwork (*i.e.*, the core) has been found, all other nodes are considered part of the periphery sub-network.

The global features we used in the REA are standard tools of such analysis and we quantified their variation with attack using an analysis of variance (ANOVA). Specifically, we used efficiency (E), betweenness centrality (BC) and degree (k) as our global network measures in the REA. While BC and k are less common in such analysis, efficiency (E) is a standard choice for network analysis under REA because it quantifies how efficiently the nodes of the network are connected (van den Heuvel and Sporns, 2011). BC and k both quantify how well-connected the majority of the nodes in the network are, though each measure quantifies this in a different way. For a full description of these and other network measures, the reader is referred to other comprehensive descriptions (Rubinov and Sporns, 2010). For the ANOVA, we compared E, BC and k of each subject's sub-networks (core and periphery) during REA for each trial category (see Fig. 2C for examples of these networks). We did so for sub-networks, rather than whole networks, so that the more robust core would not dominate the analysis by chance during the REA. Thus, we performed a two-way repeated measures ANOVA with subject as the random variable (*trial category* × *edge attack*) for E, BC and k.

Network feature analysis: elastic net regularized discrimination by trial category

We also trained and tested an elastic net regularized logistic regression classifier on each trial category's network measures, using leave-one-subject-out cross validation (illustrated in Fig. 3). As with the post-stimulus BOLD PEs, we calculated AUC with leave-one-subject out cross validation. The use of the elastic net has the effect of reducing potential sources of noise in the discrimination. We implemented the elastic net in our logistic regression (Conroy and Sajda, 2012) by performing a parameter sweep of the sparsity parameter (α) on {0,0.1:0.2:0.5}, where no sparsity in the solution means that $\alpha = 0$. When no sparsity was used, a simple evaluation of the AUC was our classification metric. But when sparsity was used, we followed the approach of Conroy et al. (Conroy and Sajda, 2012; Conroy et al., 2013) to pick the optimum solution on the Pareto frontier trading off AUC and consistent selection of the same features (an example of a Pareto frontier is shown in the Supplementary data in Fig. S2). The second parameter for elastic net (λ) was determined with an algorithm based on degrees of freedom in the solution space (Park and Hastie, 2008). In the Pareto space, the optimum point is that closest to (1,1), indicating an AUC of 1 and probability of selecting the same features of 1.

This Pareto optimal criterion was used as the classification metric, though in the Results we quote the AUC and accuracy values. Regardless of the classification metric used (*i.e.*, AUC

or Pareto optimality), we calculated p-values *via* permutations of the trial category labels (10,000 permutations). All classification results are reported at $p < 0.05$.

Network feature analysis: discrimination sensitivity by feature

We analyzed the sensitivity of our Pareto optimal classifiers by removing one feature at a time, retraining the classifier and recalculating the accuracy of the discriminating component. This was done with leave-one-subject-out cross validation. Such a technique is based on a feature ranking protocol applicable to any classifier (Chang and Lin, 2008), and we adapt it here for linear logistic regression classifiers.

Having a new accuracy value for each removed feature, we calculated the relative change in accuracy ((new-original)/original) for each feature. We define a measure that drives classification as one that upon removal causes a negative relative change in accuracy after classifier retraining.

While such an analysis did not provide insight into the sensitivity of the interactions between features, it does provide insight into each feature on its own. Since feature values are related to each other *via* the trial category network structure, the shortcoming of such a technique was negligible compared to the computational savings from performing combinatorial sums of all network measures.

Finally, we also correlated the discriminating component with each feature to test classifier sensitivity. Due to multiple comparisons across features, we corrected using the false discovery rate (FDR) and set a threshold of $p = 0.05$ for significant correlations. This method allowed us an alternative way to examine each feature's impact on the classifier, but without removing that feature from the calculation.

Control analyses demonstrating utility of network approach

We ran extensive control analyses to determine the impact our network-based approach had on discrimination of task performance based on pre-stimulus measures. For example, for sub-network discrimination, we examined the role of core/periphery breakdowns. First, we considered whether core/periphery membership alone drove discrimination. Second, we considered whether the repeated information of one node being in the core and consequently *not* being in the periphery (or *vice versa*) drove discrimination. For whole network discrimination, we considered whether it was possible to classify pre-stimulus trial category networks using mean BOLD values in isolation, *i.e.*, with disregard to the edges of the network.

Results

Network node construction from brain parcellation

The searchlight analysis revealed a network of 57 nodes covering task-related parts of the cortex, subcortex, cerebellum and part of the brain stem (Fig. 4; full table of node numbers and their anatomical regions is provided in Supplementary data).

The corresponding p-values of each node-center are shown *via* the color bar as well. The largest contributors of nodes across the anatomy were as follows: lateral occipital cortex sensorimotor cortical areas, the frontal cortex, parts of the cerebellum/brainstem, and sub-cortical motor control areas, such as the putamen and thalamus. The MNI coordinates listed with each node in Supplementary data (Table S2) provide details how each significant node is distributed within these brain regions having differing sizes, shapes and functions.

Random edge attack analysis: pre-stimulus functional connectivity varies by trial category

The random edge attack (REA) analysis revealed high sensitivity in periphery sub-network efficiency and low sensitivity in core subnetwork efficiency. The REA also showed minimal sensitivity in whole network efficiency to when attack was limited to either core or periphery nodes, though attacks to the core trended toward greater sensitivity. We summarize these results for each trial category and normalize by baseline efficiency for ease of comparison (see Fig. S1 in Supplementary data). Standard error bars, which are small, indicate error about the mean obtained from the 500 REAs. These trends in efficiency change from REA in the core and periphery are similar to those seen in other such attacks on high- and low-degree networks, respectively (Crucitti et al., 2004).

To better quantify the differences seen in Fig. S1, we performed a two-way repeated measures ANOVA with subject as the random variable (trial category × edge attack), we found significant main effects for trial category in E (efficiency), k (degree) and BC (betweenness centrality) of both sub-networks. We summarize these results in Table 1 and show these trends for k, BC and E in Fig. 5, having normalized by the baseline to compare across network measures. Error bars in Fig. 5 indicate standard error of the mean from each subject's REA analysis. As expected, we also see a strong main effect of edge attack, but we see no significant interaction for trial category with attack, indicating that trial category shows a global effect on both core and periphery subgraphs, regardless of the number of edges attacked.

Particularly noteworthy from this analysis is how these measures are affected by attack on the periphery sub-network. Specifically attack on the periphery network of Correct No-Go (P_{CNG}) shows the greatest effect on k, BC and E. This is important because it is the only inhibition response of the three trial categories, indicating that the more fragile periphery network is likely a strong mediator of the inhibition response.

Elastic net classification by trial category

Using the elastic net, we found that we could classify trial categories by pre-stimulus whole or sub-network measures. Results are summarized in Table 2.

Whole networks distinguished N_{CG} from N_{CNG} and N_{CNG} from N_{ING} networks. In particular, we performed N_{CG} *vs.* N_{CNG} network discrimination with a leave-one-subject-out accuracy of 0.77, AUC = 0.87 ($p < 0.01$) and the N_{CNG} *vs.* N_{ING} discrimination with a leave-one-subject-out accuracy of 0.91, AUC = 0.91 ($p = 0.01$). The N_{CG} *vs.* N_{ING} discrimination was not significant at AUC = 0.60 ($p > 0.20$).

Sub-networks distinguished the N_{CG} from N_{ING} networks, though for the analysis they had been divided into (C_{CG}, P_{CG}) and (C_{ING}, P_{ING}) sub-networks. In particular, we could discriminate these sub-networks with an accuracy of 0.77, AUC = 0.77 ($p < 0.03$). Classification of (C_{CNG}, P_{CNG}) *vs.* (C_{ING}, P_{ING}) sub-networks was also significant (AUC = 0.77, $p = 0.03$), though this was not an improvement of the AUC from what was found earlier with whole networks. We did not find significant discrimination in N_{CG} *vs.* N_{CNG} *via* their sub-networks.

Elastic net classification sensitivity analysis

We tested the impact of each feature on the classification using the sensitivity analysis described in the Materials and methods. Recall, that we define feature importance as the relative change in classification accuracy when the classifier is re-trained without that individual feature. More important features will thus result in lower classification accuracy when they are individually removed. Using this criterion, we found that only a small number of features individually drove the classification on whole networks. One feature (BC_9) drove the N_{CG} *vs.* N_{CNG} network discrimination and three features (BC_9, BC_{10}, and BC_{26}) drove that of N_{CNG} *vs.* N_{ING}, all of which are shown in Fig. 6. For sub-network discrimination, seventeen BC-based features individually drove classification, more of these features coming from periphery than from core sub-networks. The top six features that drove the N_{CG} *vs.* N_{ING} network discrimination (core: BC_{15}, periphery: BC_{48}, BC_{16}, BC_{25}, BC_{42}, BC_{56}) are shown in Fig. 6.

To further quantify the impact of each feature on classification, we considered significant feature correlations with the discriminating component. We found that BC_9 significantly correlated ($p < 0.05$, FDR corrected) with the discriminating component (y) for both N_{CG} *vs.* N_{CNG} and N_{CNG} *vs.* N_{ING} discriminations (see insets A and B to Fig. 6). In particular, we found from these results that low values of BC_9 indicate discrimination for upcoming motor-response trials (*e.g.*, CG or ING), while high values of BC_9 indicate discrimination for upcoming motor-inhibition trials (*e.g.*, CNG). These results demonstrated the importance of the network node on the right putamen (#9) for each of these trial category discriminations.

When indexed onto the underlying anatomy, the most sensitive nodes reveal a network of structures whose values of betweenness centrality are crucial to discriminating pre-stimulus trial category neural states. We show these nodes color-coded by primary color addition rules in Fig. 7.

Using this approach, we found that the BC of the right putamen (#9) most strongly drives the N_{CG} *vs.* N_{CNG} discrimination, whereas the BC of the right putamen (#9), left LOC (#10) and left thalamus (#26) most strongly drive the N_{CNG} *vs.* N_{ING} discrimination. After core/periphery sub-network breakdown, we also found that the BC of the supplementary motor area, or SMA, (#15) when it was in the core, the left putamen (#16), left occipital pole and LOC (#25), left frontal pole (#42), right frontal pole (#48) and right inferior temporal gyrus, or ITG, (#56) when they were each in the periphery most strongly drive the N_{CG} *vs.* N_{ING} discriminations.

Control analyses showing importance of network approach

We also checked how vital the network measures were to trial category discrimination. In particular, we trained our classifier on mean BOLD data of each trial category using all 57 nodes found from the searchlight. We found that we could discriminate CG *vs.* CNG at AUC = 0.68 (p = 0.10), CNG *vs.* ING at AUC = 0.78 (p = 0.03), and CG *vs.* ING at AUC = 0.65 (p = 0.14). If we compare these results to what was found with either whole network or sub-network measures we see that the use of these measures improved our AUC for each trial category: AUC = 0.87 for CG *vs.* CNG, AUC = 0.91 for CNG *vs.* ING, and AUC = 0.77 for CG *vs.* ING. Even though the discrimination of CNG *vs.* ING is significant without them, we found a substantial improvement when network measures were included. These results demonstrate the utility of the network measures in discriminating pre-stimulus activity for each trial category across the brain.

Discussion

The objective of this research was to investigate how whole-brain network constructs, representing pre-stimulus brain state, modulate task performance. To meet this objective, we utilized fMRI BOLD imaging and used a graph-based approach to construct networks characterizing pre-stimulus functional connectivity across the brain. We developed a searchlight analysis driven by post-stimulus BOLD changes in behaviorally correct and incorrect trials that allowed us to isolate functional nodes in the brain for the READ-M task. This analysis revealed distributed anatomical networks whose pre-stimulus configuration was a major determiner of task performance across subjects. We contextualize these findings in the relevant literature below.

Searchlight analysis reveals task relevant neural substrates

A challenge for functional connectivity analysis is the combinatorial explosion in the number of possible connections (*e.g.* graph edges) between areas (*e.g.* nodes) (Bressler and Menon, 2010; Sporns, 2011). For instance, the $2 \times 2 \times 2$ mm^3 BOLD images we collected contain over 100,000 voxels. Without paring down the node-space, *i.e.*, parcellation, the edge-space becomes unmanageable. A variety of parcellation techniques exist based on anatomical methods (Desikan et al., 2006; Eickhoff et al., 2005; Tzourio-Mazoyer et al., 2002). The choice of parcellation technique has been shown to affect multiple topological parameters of the resulting networks (Bullmore and Sporns, 2009; Wang et al., 2009). For resting state fMRI (rs-fMRI), consistency of node boundaries is a criterion that drives the choice of parcellation algorithm (Shen et al., 2010). However for a task-based experimental design, we can exploit stimulus and response data to constrain our parcellation strategy—*i.e.* utilizing a searchlight analysis to reduce the node-space in a principled manner. Our parcellation criterion was that the 12 mm volume around a node's center voxel should be highly discriminative for behavioral outcome based on the BOLD signal parameter estimates (PEs) found during stimulus presentation. Using this approach, we found 57 nodes across the brains of our subjects that drove behavioral performance outcome in our READ-M baseball paradigm.

The 57 nodes identified using our searchlight approach covered anatomical structures linked *via* other studies to constituent processes likely employed for our READ-M paradigm. For example, bilateral LOC contained the most nodes (1, 4, 5, 6, 10, 18, 22, 25, 36, and 37) where LOC has been shown to play an important role in object recognition (Ferber et al., 2003; Grill-Spector et al., 2001). The prevalence of LOC-situated nodes could indicate that subjects' behavioral success is based on their ability to recognize the trajectory as an object and/or categorical event. Interestingly, LOC has more contributing nodes than MT, which is known to be important for motion perception (El-Shamayleh et al., 2010; O'Keefe and Movshon, 1998). In our parcellation a limited number of nodes in MT are significant (39, 55, 57), which may imply that motion tracking is less important for behavioral success than object/event recognition. Nevertheless, the LOC is volumetrically larger than MT and so this result may be a function of anatomical volume, instead of task-relevance. An experimental design that compares all-at-once trajectory presentation with the time-evolving stimulus presentation used here would be a way to resolve the issue.

For task success, motion analysis and object recognition do not happen in isolation. Rather, these perceptual/cognitive operations must link with an appropriate motor program, *i.e.*, response or inhibition of response. After the LOC, it is the motor and somatosensory cortices that show the most significant nodes (2, 3, 7, 13, 15, 29, 30, 35, and 47). These cortical areas control overt movement (Binkofski et al., 2002; Meier et al., 2008), planned movement (Gerloff et al., 1997; Picard and Strick, 2003; Roland et al., 1980), and somatosensory input/feedback (Craig, 1999; Van Boven and Johnson, 1994), all of which serve a vital role in correct behavioral response execution. Due to their proximity to the scalp, the neural activity of these areas is more suitable for measurement with non-invasive EEG/MEG imaging techniques. Consequently, pre-stimulus modulation of upcoming task performance based on these imaging modalities relies heavily on these and other cortical substrates (Linkenkaer-Hansen et al., 2004; Zhang et al., 2008). However, with fMRI BOLD imaging, we also can identify sub-cortical structures, which project to sensorimotor and other areas (Theyel et al., 2010; Viaene et al., 2011). We find that two such subcortical motor substrates (the putamen and the thalamus) appear in our upper third of nodes (9, 16), one in the middle third (26) and one in the final third (41). Previous work has shown that these areas are not only important for motor response (Alexander and Crutcher, 1990; DeLong et al., 1984) but also anticipation (Guitart-Masip et al., 2011; Kurniawan et al., 2013).

The final two large contributors to the node distribution were substrates in the cerebellum/brainstem and the frontal cortices. The cerebellum/brainstem contained seven nodes (8, 11, 17, 24, 28, 33,50). The incorporation of the cerebellum in this analysis is a substantial benefit of using fMRI BOLD imaging, as opposed to EEG/MEG, because of the cerebellum's vital role in coordinating movement (Apps and Garwicz, 2005; Doya, 2000). Pre-stimulus techniques based on EEG/MEG lack the ability to measure this important contributor to movement coordination due depth, the high frequency range of cerebellar activity and possible neck movement confounds (Dalal et al., 2013). The frontal cortices, alternatively, are closer to the scalp and so source localization algorithms can suitably model activity originating from these regions based on medium-density scalp-level measurements.

Nevertheless, we find that frontal cortices, substrates linked to planning and executive decision-making (Koechlin and Hyafil, 2007), contain a comparable number of nodes to the cerebellum/brainstem (20, 21, 42, 46, 48, 51, 53, and 54) discriminating behaviorally correct and incorrect trials. Based on the prevalence of significant nodes, we conclude that, while the BOLD signal of frontal cortices carries discriminative information between correct and incorrect trials, they are less discriminative by volume than areas processing object recognition and motor response commission, inhibition and coordination. Such a result extends previous work that we have done on a paradigm similar to our READ-M paradigm, in which we found cortical source differences between behaviorally correct and incorrect trials originating in the left frontal cortex (Sherwin et al., 2012). The searchlight analysis completes this original spatial picture, finding significantly discriminating areas by their p-value, covering sensorimotor, LOC, subcortical motor and cerebellar/brainstem substrates.

Prominent drivers of pre-stimulus neural modulators of behavioral performance

While the searchlight analysis significantly reduced the dimensionality of the node-space, the REA and classification results still utilized a 57-node space connected by mean = 639, SE = 20 edges. The REA is a technique for probing global features of a network's connectivity (Achard et al., 2006; van den Heuvel and Sporns, 2011). With it, we determined that trial category showed significant main effects in both core and periphery sub-networks by different though significant amounts (Table 1).

However the REA alone could not predict pre-stimulus modulation of upcoming task performance. To this end, we summarized this high-dimensional feature space with network measures such as degree (k), betweenness centrality (BC), and the others listed in Table S1. These measures have been used extensively in graph theoretic approaches to brain connectivity (Bullmore and Sporns, 2009; Rubinov and Sporns, 2010). Using these measures, we trained and tested a linear classifier on node connectivity properties, rather than on isolated node response properties. In fact, our control analyses show the additional classification value on using these network level measures (see Supplementary data). We used a sensitivity analysis to investigate how an individual node's connectivity properties impacted trial category discrimination (Chang and Lin, 2008). Despite more elaborate procedures for sensitivity analysis, such as Sequential Forward Floating Search (Pudil and Kittler, 1994; Sun et al., 2005), the single-node technique we employed provided a suitable tradeoff between computation time (high for algorithms like SFFS) and feature interaction (already incorporated into network measures by definition).

With the sensitivity analysis, we determined that the pre-stimulus connectivity of the right putamen plays an important role in modulating behavioral outcome. In particular, the BC of this node (9) is high for upcoming response inhibitions and low for commissions (see insets to Fig. 6). Recall, that the definition of BC is that it is the number of the shortest paths from all vertices to all other vertices passing through a given node (Rubinov and Sporns, 2010). Consequently, a high number of shortest functional paths through node 9 mediate response inhibition; *vice versa* for response commission. This means that response commission involves less immediate functional connectivity to the putamen than inhibition. A possible interpretation of this result is that anticipation of a successful action (which we might view

as a type of implicit 'reward') locally drives commission decisions *via* the putamen, while cortical feedback mitigates such anticipation during inhibition, for instance, *via* the fronto-parietal inhibition network (Dodds et al., 2011; Kawashima et al., 1996).

The centrality of the right putamen to both correct inhibition discriminations (CG *vs.* CNG, CNG *vs.* ING) highlights its differing role in correct and incorrect response commissions. When discriminating Correct Go (CG) from Correct No-Go (CNG), the right putamen BC is the only feature driving discrimination, determined by our sensitivity analysis. When discriminating Correct No-Go (CNG) from Incorrect No-Go (ING), the right putamen is the strongest driver of discrimination, showing a 46% reduction in classification accuracy when removing it. However two other nodes largely drive discrimination of CNG *vs.* ING networks: the left thalamus (10) and left LOC (26). Succinctly, behaviorally correct decisions that are either commissions or inhibitions differ only in the network's regulation of the right putamen. But behaviorally correct inhibitions differ from incorrect commissions, not only in network regulation of the right putamen but also, *via* functional proximity of other subcortical motor (left thalamus) and object recognition (left LOC) substrates. Lesion studies in humans or invasive brain imaging studies in primates would allow experimental testing of this interpretation, but such work is beyond the scope of this study.

Discrimination of response commission pre-stimulus networks by behavioral accuracy proved the most difficult (*i.e.*, CG *vs.* ING discrimination). To discriminate these networks we utilized the k-core decomposition algorithm to recursively prune nodes into core and periphery sub-networks (Carmi et al., 2007). As Fig. 5 demonstrated, core and periphery sub-networks displayed different global properties during REA, with core sub-networks expectedly showing less sensitivity to attack than periphery (Crucitti et al., 2004). This means that a separation of the whole network into core and periphery components would provide more information to a classifier, though this comes at the price of adding more noise on a feature level. We see this effect in the sensitivity analysis summary of Fig. 6, where the sub-network breakdown of CG *vs.* ING networks generated seventeen features driving classification, compared to three (CNG *vs.* ING) and one feature (CG *vs.* CNG).

The top driving features discriminating behavioral accuracy in response commission networks indicated more distributed differences than those involving response inhibition. Seventeen features drove this discrimination, *versus* three and one for the previous. In Fig. 6, we considered the top six such features. The removal of the BC of the 48th node as part of the periphery sub-network in the right frontal pole resulted in a 30% reduction in leave-one-subject-out accuracy. The removal of the BC of the 15th node as part of the core in the SMA and that of the 16th node as part of the periphery in the left putamen resulted in nearly a 20% reduction in accuracy. Finally, the removal of the BC of the 25th node in LOC, that of the 42nd node in the frontal cortex and that of the 56th node in the right ITG, all as part of the periphery subnetwork, resulted in more than a 10% reduction in accuracy.

Taking the magnitude of reduction in accuracy as a metric of feature importance, we can speculate that these neural substrates contribute in this way to behavioral accuracy on commission trials. Following this logic, the right frontal pole's pre-stimulus centrality to adjacent periphery nodes is of paramount importance to behavioral accuracy on upcoming

trials. Previous work utilizing cellular and connectional anatomy has demonstrated the frontal pole's role in strategic memory recall and executive decision-making (Koechlin and Hyafil, 2007; Ramnani and Owen, 2004), in particular highlighting its role at integrating multiple cognitive operations toward the pursuit of a higher goal. Lesser reductions in accuracy were found for the BC of SMA and left putamen, both substrates heavily implicated in motor planning and execution (Theyel et al., 2010; Viaene et al., 2011), as well as reward anticipation (Haruno et al., 2004; Hayes and Greenshaw, 2011; Marsh et al., 2010). Finally, the centrality of LOC, and again the frontal cortex and ITG, implicates substrates connected to object recognition (Ferber et al., 2003; Grill-Spector et al., 2001), strategic memory recall and executive decision-making (Koechlin and Hyafil, 2007; Ramnani and Owen, 2004), and high-level visual processing (Denys et al., 2004; Gross, 1992). The sensitivity analysis in tandem with the linear classifier allows us to characterize the interaction between these neural substrates, which in isolation have been shown to characterize component cognitive functions to the READ-M task performed here. Although previous studies have shown these individual areas to be important components for high-level visual processing, reward anticipation, *etc.*, our method using a graph-based analysis of whole-brain pre-stimulus state has shown how these areas are functionally related and configured for a rapid decision making task.

Supplementary Material

Refer to Web version on PubMed Central for supplementary material.

Acknowledgments

This work was supported by grants from the Army Research Office (W911NF-11-1-0219), the National Institutes of Health (R01-MH085092), the U.S. Army Research Laboratory under Cooperative Agreement Number W911NF-10-2-0022 and in part by an appointment to the U.S. Army Research Laboratory Postdoctoral Fellowship Program administered by the Oak Ridge Associated Universities through a contract with the U.S. Army Research Laboratory. The views and conclusions contained in this document are those of the authors and should not be interpreted as representing the official policies, either expressed or implied, of the Army Research Laboratory of the U.S. Government. The U.S. Government is authorized to reproduce and distribute reprints for Government purposes notwithstanding any copyright notation herein.

References

Achard S, Salvador R, Whitcher B, Suckling J, Bullmore E. A resilient, low-frequency, small-world human brain functional network with highly connected association cortical hubs. J Neurosci. 2006; 26(1):63–72. [PubMed: 16399673]

Adair RK. The physics of baseball. Phys Today. 1995; 48 (5):26–31.

Albert R, Barabasi AL. Statistical mechanics of complex networks. Rev Mod Phys. 2002; 74(1):47–97.

Alexander GE, Crutcher MD. Preparation for movement: neural representations of intended direction in three motor areas of the monkey. J Neurophysiol. 1990; 64(1):133–150. [PubMed: 2388061]

Alvarez-Hamelin J, Dall-Asta L, Barrat A, Vespignani A. K-core decomposition of internet graph hierarchies, self-similarity and measurement biases. Netw Heterog Media. 2008; 3 (2):371–393.

Apps R, Garwicz M. Anatomical and physiological foundations of cerebellar information processing. Nat Rev Neurosci. 2005; 6(4):297–311. [PubMed: 15803161]

Armenti, A. The Physics of Sports. Vol. 1. American Institute of Physics; New York: 1992.

Benjamini YHY. Controlling the false discovery rate: a practical and powerful approach to multiple testing. J R Stat Soc Ser B Methodol. 1995; 57(1):289–300.

Binkofski F, Fink GR, Geyer S, Buccino G, Gruber O, Shah NJ, Taylor JG, Seitz RJ, Zilles K, Freund HJ. Neural activity in human primary motor cortex areas 4a and 4p is modulated differentially by attention to action. J Neurophysiol. 2002; 88(1):514–519. [PubMed: 12091573]

Bjornsdotter M, Rylander K, Wessberg J. A Monte Carlo method for locally multivariate brain mapping. Neuro Image. 2011; 56 (2):508–516. [PubMed: 20674749]

Brainard DH. The psychophysics toolbox. Spat Vis. 1997; 10(4):433–436. [PubMed: 9176952]

Bressler SL, Menon V. Large-scale brain networks in cognition: emerging methods and principles. Trends Cogn Sci. 2010; 14(6):277–290. [PubMed: 20493761]

Bullmore E, Sporns O. Complex brain networks: graph theoretical analysis of structural and functional systems. Nat Rev Neurosci. 2009; 10(3):186–198. [PubMed: 19190637]

Carmi S, Havlin S, Kirkpatrick S, Shavitt Y, Shir E. A model of Internet topology using k-shell decomposition. Proc Natl Acad Sci U S A. 2007; 104(27):11150–11154. [PubMed: 17586683]

Chang, Y-W.; Lin, C-J. SVM. 2008. Feature ranking using linear; p. 53-64.

Conroy B, Sajda P. Fast, exact model selection and permutation testing for l-regularized logistic regression. JMLR Workshop Conf Proc. 2012; 22:246–254. [PubMed: 24382986]

Conroy BR, Walz JM, Sajda P. Fast bootstrapping and permutation testing for assessing reproducibility and interpretability of multivariate fMRI decoding models. PLoS ONE. 2013; 8 (11):e79271. [PubMed: 24244465]

Craig JC. Grating orientation as a measure of tactile spatial acuity. Somatosens Mot Res. 1999; 16(3): 197–206. [PubMed: 10527368]

Crucitti P, et al. Error and attack tolerance of complex networks. Phys A. 2004; 340:388–394.

Dalal SS, Osipova D, Bertrand O, Jerbi K. Oscillatory activity of the human cerebellum: the intracranial electrocerebellogram revisited. Neurosci Biobehav Rev. 2013; 37(4):585–593. [PubMed: 23415812]

Dale AM. Optimal experimental design for event-related fMRI. Hum Brain Mapp. 1999; 8(2–3):109–114. [PubMed: 10524601]

DeLong MR, Alexander GE, Georgopoulos AP, Crutcher MD, Mitchell SJ, Richardson RT. Role of basal ganglia in limb movements. Hum Neurobiol. 1984; 2(4):235–244. [PubMed: 6715208]

Denys K, Vanduffel W, Fize D, Nelissen K, Peuskens H, Van Essen D, Orban GA. The processing of visual shape in the cerebral cortex of human and nonhuman primates: a functional magnetic resonance imaging study. J Neurosci. 2004; 24(10):2551–2565. [PubMed: 15014131]

Desikan RS, Segonne F, Fischl B, Quinn BT, Dickerson BC, Blacker D, Buckner RL, Dale AM, Maguire RP, Hyman BT, et al. An automated labeling system for subdividing the human cerebral cortex on MRI scans into gyral based regions of interest. Neuro Image. 2006; 31 (3):968–980. [PubMed: 16530430]

Dodds CM, Morein-Zamir S, Robbins TW. Dissociating inhibition, attention, and response control in the frontoparietal network using functional magnetic resonance imaging. Cereb Cortex. 2011; 21 (5):1155–1165. [PubMed: 20923963]

Doya K. Complementary roles of basal ganglia and cerebellum in learning and motor control. Curr Opin Neurobiol. 2000; 10(6):732–739. [PubMed: 11240282]

Eickhoff SB, Stephan KE, Mohlberg H, Grefkes C, Fink GR, Amunts K, Zilles K. A new SPM toolbox for combining probabilistic cytoarchitectonic maps and functional imaging data. Neuro Image. 2005; 25 (4):1325–1335. [PubMed: 15850749]

Ekman M, Derrfuss J, Tittgemeyer M, Fiebach CJ. Predicting errors from reconfiguration patterns in human brain networks. Proc Natl Acad Sci U S A. 2012; 109(41):16714–16719. [PubMed: 23012417]

El-Shamayleh Y, Kiorpes L, Kohn A, Movshon JA. Visual motion processing by neurons in area MT of macaque monkeys with experimental amblyopia. J Neurosci. 2010; 30(36):12198–12209. [PubMed: 20826682]

Ferber S, Humphrey GK, Vilis T. The lateral occipital complex subserves the perceptual persistence of motion-defined groupings. Cereb Cortex. 2003; 13 (7):716–721. [PubMed: 12816886]

Garas A, Schweitzer F, Havlin S. A k-shell decomposition method for weighted networks. New J Phys. 2012:083030.

Gerloff C, Corwell B, Chen R, Hallett M, Cohen LG. Stimulation over the human supplementary motor area interferes with the organization of future elements in complex motor sequences. Brain. 1997; 120 (Pt 9):1587–1602. [PubMed: 9313642]

Grill-Spector K, Kourtzi Z, Kanwisher N. The lateral occipital complex and its role in object recognition. Vis Res. 2001; 41(10–11):1409–1422. [PubMed: 11322983]

Gross CG. Representation of visual stimuli in inferior temporal cortex. Philos Trans R Soc Lond B Biol Sci. 1992; 335(1273):3–10. [PubMed: 1348134]

Guitart-Masip M, Fuentemilla L, Bach DR, Huys QJ, Dayan P, Dolan RJ, Duzel E. Action dominates valence in anticipatory representations in the human striatum and dopaminergic midbrain. J Neurosci. 2011; 31(21):7867–7875. [PubMed: 21613500]

Hanslmayr S, Aslan A, Staudigl T, Klimesch W, Herrmann CS, Bauml KH. Prestimulus oscillations predict visual perception performance between and within subjects. Neuro Image. 2007; 37 (4): 1465–1473. [PubMed: 17706433]

Hartstra E, Oldenburg JF, Van Leijenhorst L, Rombouts SA, Crone EA. Brain regions involved in the learning and application of reward rules in a two-deck gambling task. Neuropsychologia. 2010; 48 (5):1438–1446. [PubMed: 20105435]

Haruno M, Kuroda T, Doya K, Toyama K, Kimura M, Samejima K, Imamizu H, Kawato M. A neural correlate of reward-based behavioral learning in caudate nucleus: a functional magnetic resonance imaging study of a stochastic decision task. J Neurosci. 2004; 24(7):1660–1665. [PubMed: 14973239]

Hasson U, Ghazanfar AA, Galantucci B, Garrod S, Keysers C. Brain-to-brain coupling: a mechanism for creating and sharing a social world. Trends Cogn Sci. 2012; 16(2):114–121. [PubMed: 22221820]

Hayes DJ, Greenshaw AJ. 5-HT receptors and reward-related behaviour: a review. Neurosci Biobehav Rev. 2011; 35(6):1419–1449. [PubMed: 21402098]

Hesselmann G, Kell CA, Kleinschmidt A. Ongoing activity fluctuations in hMT+ bias the perception of coherent visual motion. J Neurosci. 2008; 28(53):14481–14485. [PubMed: 19118182]

Honey CJ, Kotter R, Breakspear M, Sporns O. Network structure of cerebral cortex shapes functional connectivity on multiple time scales. Proc Natl Acad Sci U S A. 2007; 104(24):10240–10245. [PubMed: 17548818]

Honey CJ, Sporns O, Cammoun L, Gigandet X, Thiran JP, Meuli R, Hagmann P. Predicting human resting-state functional connectivity from structural connectivity. Proc Natl Acad Sci U S A. 2009; 106(6):2035–2040. [PubMed: 19188601]

Hsieh PJ, Colas JT, Kanwisher NG. Pre-stimulus pattern of activity in the fusiform face area predicts face percepts during binocular rivalry. Neuropsychologia. 2012; 50 (4):522–529. [PubMed: 21952195]

Kamada T, Kawai S. An algorithm for drawing general undirected graphs. Inf Process Lett. 1989; 31:7–15.

Kawashima R, Satoh K, Itoh H, Ono S, Furumoto S, Gotoh R, Koyama M, Yoshioka S, Takahashi T, Takahashi K, et al. Functional anatomy of GO/NO-GO discrimination and response selection—a PET study in man. Brain Res. 1996; 728(1):79–89. [PubMed: 8864300]

Koechlin E, Hyafil A. Anterior prefrontal function and the limits of human decision-making. Science. 2007; 318 (5850):594–598. [PubMed: 17962551]

Kriegeskorte N, Goebel R, Bandettini P. Information-based functional brain mapping. Proc Natl Acad Sci U S A. 2006; 103(10):3863–3868. [PubMed: 16537458]

Kurniawan IT, Guitart-Masip M, Dayan P, Dolan RJ. Effort and valuation in the brain: the effects of anticipation and execution. J Neurosci. 2013; 33(14):6160–6169. [PubMed: 23554497]

Linkenkaer-Hansen K, Nikulin VV, Palva S, Ilmoniemi RJ, Palva JM. Prestimulus oscillations enhance psychophysical performance in humans. J Neurosci. 2004; 24(45):10186–10190. [PubMed: 15537890]

Marsh R, Hao X, Xu D, Wang Z, Duan Y, Liu J, Kangarlu A, Martinez D, Garcia F, Tau GZ, et al. A virtual reality-based fMRI study of reward-based spatial learning. Neuropsychologia. 2010; 48 (10):2912–2921. [PubMed: 20570684]

McFarlin DR, Kerr DL, Nitschke JB. Upsampling to 400-ms resolution for assessing effective connectivity in functional magnetic resonance imaging data with Granger causality. Brain Connect. 2013; 3(1):61–71. [PubMed: 23134194]

McIntosh AR. Mapping cognition to the brain through neural interactions. Memory. 1999; 7 (5–6): 523–548. [PubMed: 10659085]

McIntosh AR, Nyberg L, Bookstein FL, Tulving E. Differential functional connectivity of prefrontal and medial temporal cortices during episodic memory retrieval. Hum Brain Mapp. 1997; 5(4): 323–327. [PubMed: 20408236]

Meier JD, Aflalo TN, Kastner S, Graziano MS. Complex organization of human primary motor cortex: a high-resolution fMRI study. J Neurophysiol. 2008; 100(4):1800–1812. [PubMed: 18684903]

Muraskin, J.; Sherwin, J.; Sajda, P. A system for measuring the neural correlates of baseball pitch recognition and its potential use in scouting and player development. MIT Sloan Sports Analytics Conference; Boston, MA, USA. 2013.

O'Keefe LP, Movshon JA. Processing of first- and second-order motion signals by neurons in area MT of the macaque monkey. Vis Neurosci. 1998; 15(2):305–317. [PubMed: 9605531]

Park MY, Hastie T. Penalized logistic regression for detecting gene interactions. Biostatistics. 2008; 9 (1):30–50. [PubMed: 17429103]

Park H, Rugg MD. Prestimulus hippocampal activity predicts later recollection. Hippocampus. 2010; 20 (1):24–28. [PubMed: 19499585]

Pelli DG. The VideoToolbox software for visual psychophysics: transforming numbers into movies. Spat Vis. 1997; 10(4):437–442. [PubMed: 9176953]

Philiastides MG, Sajda P. EEG-informed fMRI reveals spatiotemporal characteristics of perceptual decision making. J Neurosci. 2007; 27(48):13082–13091. [PubMed: 18045902]

Picard N, Strick PL. Activation of the supplementary motor area (SMA) during performance of visually guided movements. Cereb Cortex. 2003; 13 (9):977–986. [PubMed: 12902397]

Pudil PNJ, Kittler J. Floating search methods in feature selection. Pattern Recogn Lett. 1994; 15(11): 1119–1125.

Ramnani N, Owen AM. Anterior prefrontal cortex: insights into function from anatomy and neuroimaging. Nat Rev Neurosci. 2004; 5(3):184–194. [PubMed: 14976518]

Roland PE, Larsen B, Lassen NA, Skinhoj E. Supplementary motor area and other cortical areas in organization of voluntary movements in man. J Neurophysiol. 1980; 43(1):118–136. [PubMed: 7351547]

Rubinov M, Sporns O. Complex network measures of brain connectivity: uses and interpretations. Neuro Image. 2010; 52 (3):1059–1069. [PubMed: 19819337]

Shen X, Papademetris X, Constable RT. Graph-theory based parcellation of functional subunits in the brain from resting-state fMRI data. Neuro Image. 2010; 50 (3):1027–1035. [PubMed: 20060479]

Sherwin J, Muraskin J, Sajda P. You can't think and hit at the same time: neural correlates of baseball pitch classification. Front Neurosci. 2012; 6:177. [PubMed: 23267311]

Shibata K, Yamagishi N, Goda N, Yoshioka T, Yamashita O, Sato MA, Kawato M. The effects of feature attention on prestimulus cortical activity in the human visual system. Cereb Cortex. 2008; 18 (7):1664–1675. [PubMed: 17991628]

Simmonds DJ, Pekar JJ, Mostofsky SH. Meta-analysis of Go/No-go tasks demonstrating that fMRI activation associated with response inhibition is task-dependent. Neuropsychologia. 2008; 46 (1): 224–232. [PubMed: 17850833]

Smith SM, Jenkinson M, Woolrich MW, Beckmann CF, Behrens TE, Johansen-Berg H, Bannister PR, De Luca M, Drobnjak I, Flitney DE, et al. Advances in functional and structural MR image analysis and implementation as FSL. Neuro Image. 2004; 23 (Suppl 1):S208–S219. [PubMed: 15501092]

Sporns O. The human connectome: a complex network. Ann N Y Acad Sci. 2011; 1224:109–125. [PubMed: 21251014]

Sun Y, Babbs CF, Delp EJ. A comparison of feature selection methods for the detection of breast cancers in mammograms: adaptive sequential floating search vs. genetic algorithm. Conf Proc IEEE Eng Med Biol Soc. 2005; 6:6532–6535. [PubMed: 17281766]

Theyel BB, Lee CC, Sherman SM. Specific and nonspecific thalamocortical connectivity in the auditory and somatosensory thalamocortical slices. Neuroreport. 2010; 21 (13):861–864. [PubMed: 20647961]

Thut G, Nietzel A, Brandt SA, Pascual-Leone A. Alpha-band electroencephalographic activity over occipital cortex indexes visuospatial attention bias and predicts visual target detection. J Neurosci. 2006; 26(37):9494–9502. [PubMed: 16971533]

Tzourio-Mazoyer N, Landeau B, Papathanassiou D, Crivello F, Etard O, Delcroix N, Mazoyer B, Joliot M. Automated anatomical labeling of activations in SPM using a macroscopic anatomical parcellation of the MNI MRI single-subject brain. Neuro Image. 2002; 15 (1):273–289. [PubMed: 11771995]

Van Boven RW, Johnson KO. The limit of tactile spatial resolution in humans: grating orientation discrimination at the lip, tongue, and finger. Neurology. 1994; 44 (12):2361–2366. [PubMed: 7991127]

van den Heuvel MP, Sporns O. Rich-club organization of the human connectome. J Neurosci. 2011; 31(44):15775–15786. [PubMed: 22049421]

Viaene AN, Petrof I, Sherman SM. Synaptic properties of thalamic input to layers 2/3 and 4 of primary somatosensory and auditory cortices. J Neurophysiol. 2011; 105(1):279–292. [PubMed: 21047937]

Wang J, Wang L, Zang Y, Yang H, Tang H, Gong Q, Chen Z, Zhu C, He Y. Parcellation-dependent small-world brain functional networks: a resting-state fMRI study. Hum Brain Mapp. 2009; 30(5): 1511–1523. [PubMed: 18649353]

Zhang Y, Wang X, Bressler SL, Chen Y, Ding M. Prestimulus cortical activity is correlated with speed of visuomotor processing. J Cogn Neurosci. 2008; 20(10):1915–1925. [PubMed: 18370597]

Appendix A. Supplementary data

Supplementary data to this article can be found online at http://dx.doi.org/10.1016/j.neuroimage.2015.01.023.

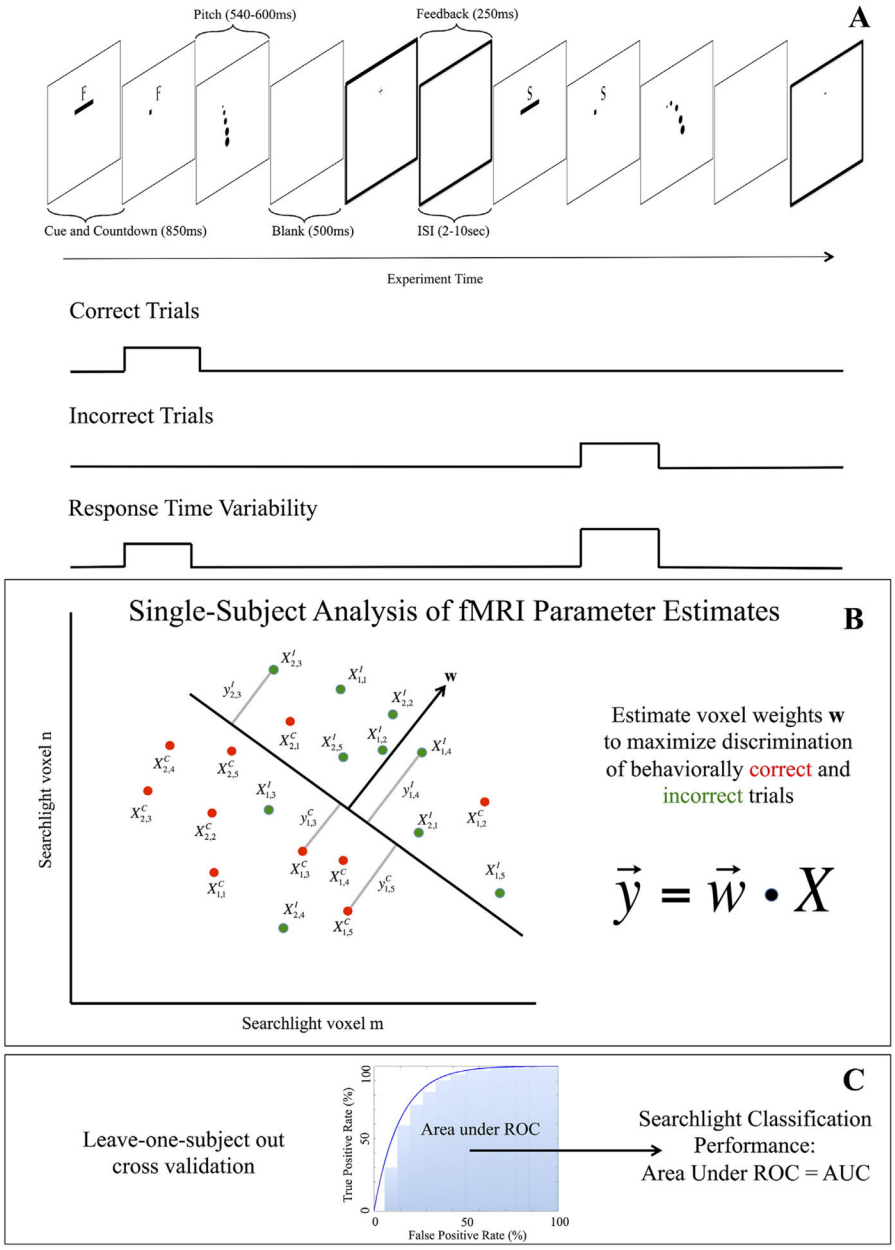

Fig. 1.

Paradigm, BOLD regressors and searchlight analysis schematics. (A) Illustration of behavioral paradigm, showing pre-stimulus cue (first trial: ‘F’ = fastball, second trial: ‘S’ = slider) and countdown, stimulus presentation as a baseball trajectory, feedback (first trial: ‘+’ = behaviorally correct, second trial:‘−’ = behaviorally incorrect) and inter-stimulus interval (ISI). Bold frames indicate time points considered to be pre-stimulus. Below, regressors indicate behaviorally correct and incorrect trials, as well as response time variability (for ‘Go’ responses). (B) Two-dimensional schematic of the searchlight analysis showing optimum discrimination between behaviorally correct and incorrect trial category

parameter estimates (two subjects, five blocks each are illustrated). (C) Illustration of leave-one-subject out cross validation to yield AUC at each searchlight center.

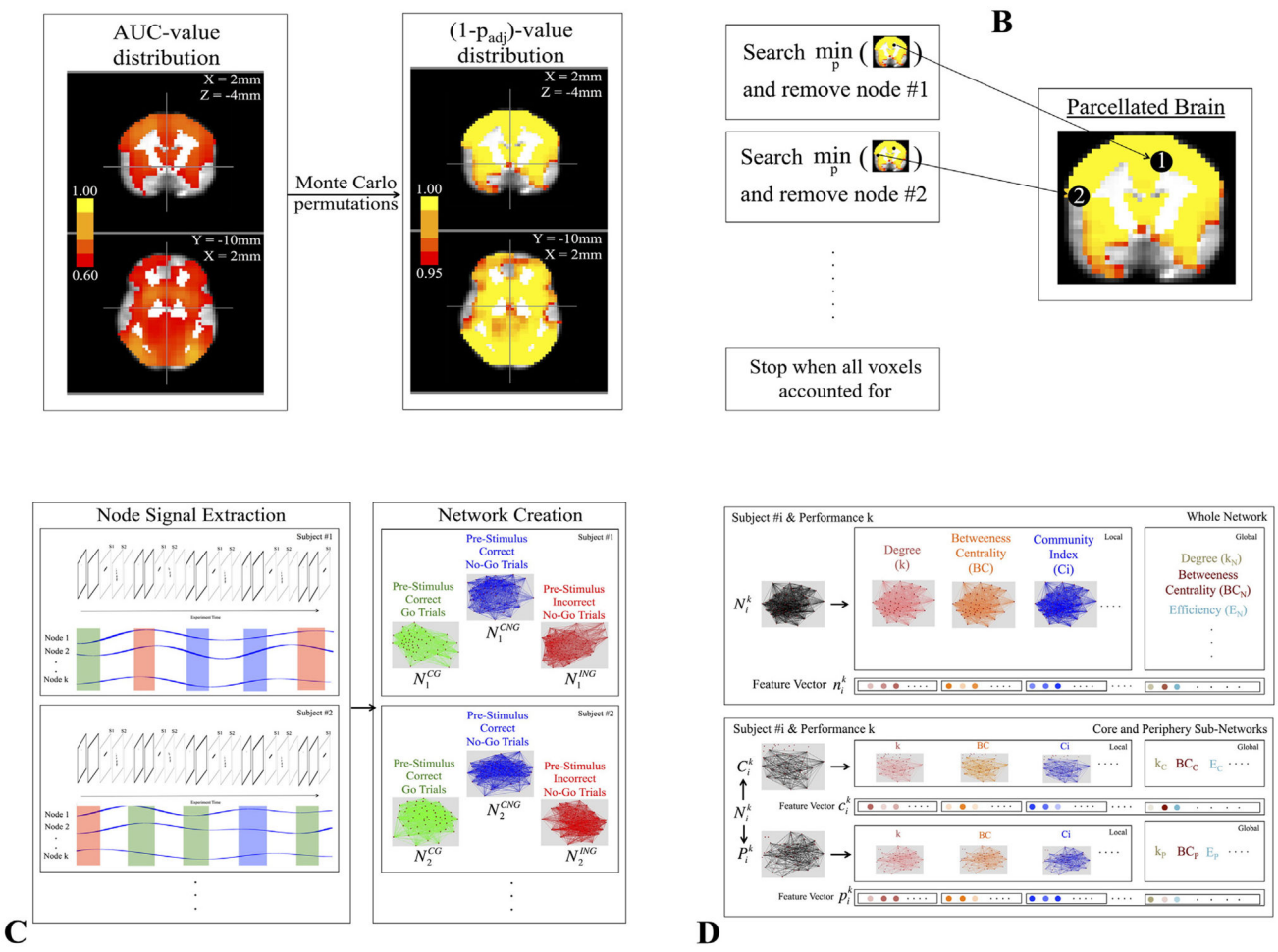

Fig. 2.

Searchlight analysis output drives brain parcellation, pre-stimulus network construction and feature calculation. (A) AUC and p-value distributions after searchlight and Monte Carlo permutations, adjusted for false discovery rate. (B) Illustration of parcellation algorithm applied to p-value distribution to generate nodes of network. (C) Schematic of pre-stimulus signal extraction from each node for Correct Go (green), Correct No-Go (blue) and Incorrect No-Go trials (red), showing the actual signal from the first five pre-stimulus intervals, which are indicated by bold frames; concatenation and thresholded correlation matrix calculation leads to trial-type-specific networks for each subject. (D) Illustration of network feature calculation from input networks; whole network and sub-network feature calculations are shown in top and bottom boxes, respectively.

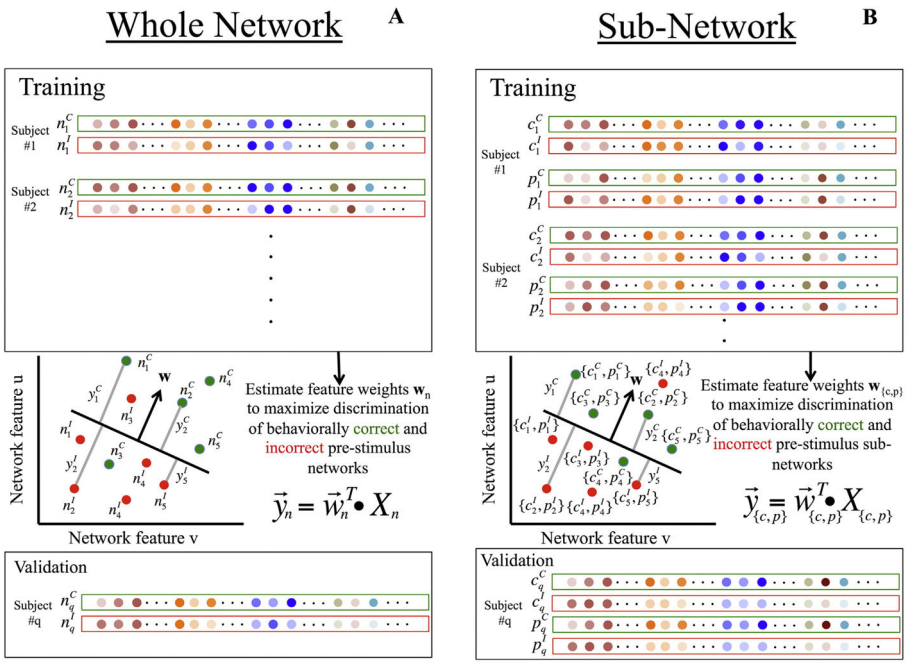

Fig. 3.

Illustration of whole and sub-network classification training and validation on behaviorally correct *vs.* behaviorally incorrect trial categories. (A) Leave-one-subject-out cross validation of whole network and (B) sub-network feature vectors. Whole network feature vectors (n) are discriminated by a classifier, w_n, and sub-network feature vectors ({c,p}) are discriminated by another classifier, $w_{\{c,p\}}$. Both classifiers are cross-validated with the left-out (qth) subject's feature vectors. The same procedure is used to classify Correct Go *vs.* Correct No-Go trial categories.

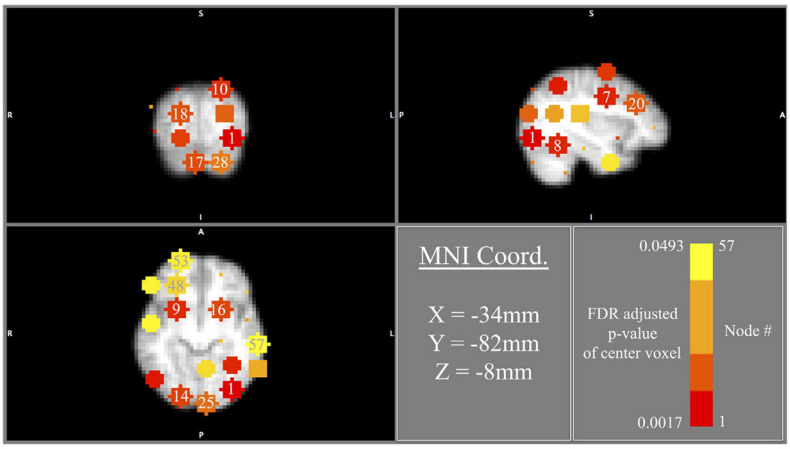

Fig. 4.

Searchlight analysis results. The searchlight analysis revealed 57 non-overlapping 12 mm-spheres, shown here in standard MNI space. All nodes are significant at a false discovery rate of $p < 0.05$ across the 24,834 voxels used in the analysis. Right (R), left (L), anterior (A), posterior (P), superior (S) and inferior (I) are indicated on each of the slices. The lower-right inset shows a color map depicting node numbers and the corresponding p-value for each node. The MNI coordinate is centered on the left lateral occipital cortex (LOC), node #1, which showed the lowest p-value for discriminating between behaviorally correct and incorrect trial categories post-stimulus. Other nodes are shown with their numbers in each view.

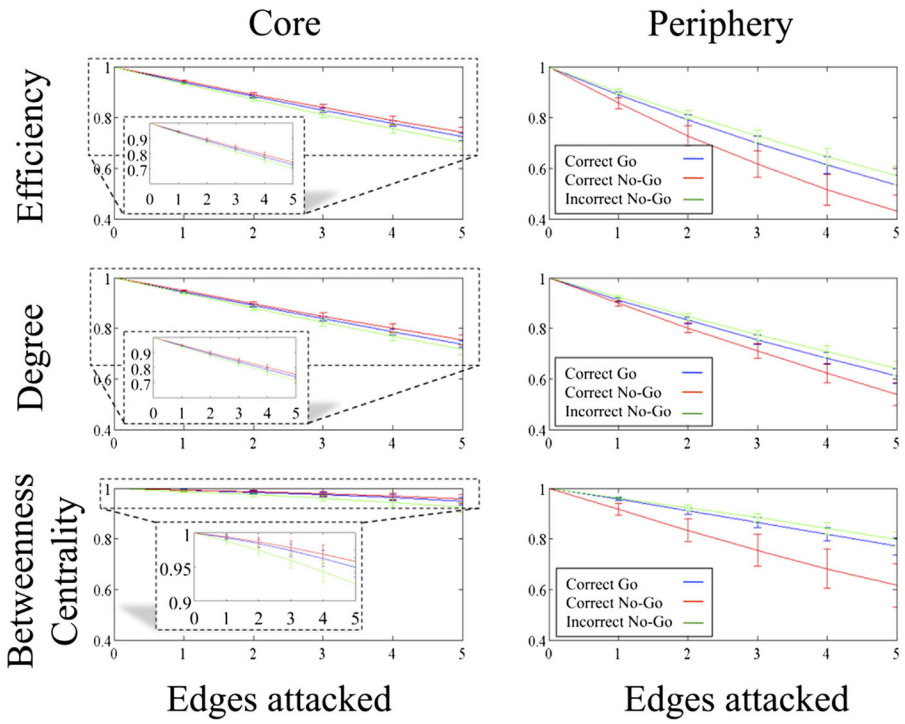

Fig. 5.

Effects of random edge attack on core and periphery sub-network measures. Trial category of each sub-network is indicated with colors (Correct Go = blue, Correct No-Go = red, Incorrect No-Go = green). Mean across all subjects' mean REA is indicated by the solid line, while error bars indicate standard error of these means across subjects. Insets for core subnetworks show zoom-in to indicated dotted-line-boxed regions.

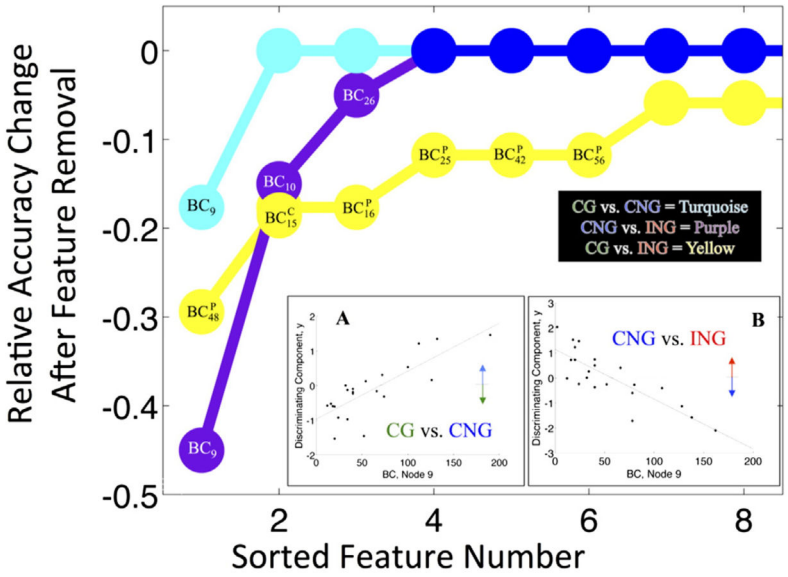

Fig. 6.

Sensitivity analysis and significant feature correlations with a discriminating component. Most sensitive features are plotted with feature name and number (*e.g.*, betweenness centrality of node #9: BC_9, core/periphery indicated by superscript). Due to space constraints, only the first eight of a total seventeen significant features are shown for Correct Go (CG) *vs.* Incorrect No-Go (ING). (A and B) Betweenness centrality of node #9 showed significant ($p < 0.05$, FDR corrected across features) correlation to the discriminating component for Correct No-Go (CNG) *vs.* Incorrect No-Go (ING) and Correct Go (CG) *vs.* Correct No-Go (CNG) discriminations. Negative values of the discriminating component indicate the first trial category and positive values indicate the second (*e.g.*, negative values in CNG *vs.* ING are for CNG, while positive values are for ING). We see from these correlations that low values of BC at node #9 anticipate a motor commission trial category (*e.g.*, CG and ING), while high values anticipate a motor inhibition trial category (*e.g.*, CNG).

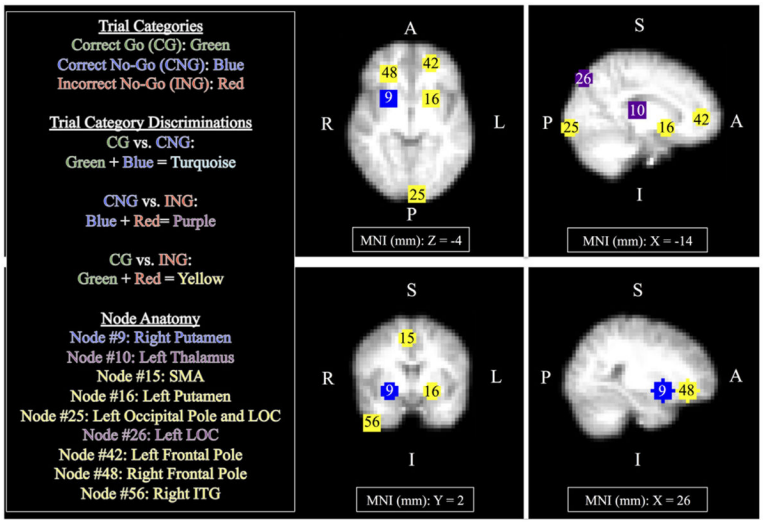

Fig. 7.

Node-measures (*i.e.*, features) driving trial category discriminations. All nodes' values of betweenness centrality drove trial category discriminations. Following the primary color coding of trial categories from Fig. 2, the inset explains how discriminations are shown as additions of primary colors (*e.g.*, Correct No-Go (blue) *vs.* Incorrect No-Go (red): blue + red = purple). When one node is common to two discriminations, the added primary colors are added once again, resulting in the common color between them (*e.g.*, purple + turquoise = blue). Anatomical structures of each node-center are shown as well.

Table 1

Two-way ANOVA (condition × attack) with subject as the random variable to assess effects on efficiency, degree and betweenness centrality of core and periphery sub-graphs.

	E_{core}	k_{core}	BC_{core}	$E_{periphery}$	$k_{periphery}$	$BC_{periphery}$
Trial category F(2,150), p > F	4.88, 0.01	4.77, 0.01	3.98, 0.02	10.43, 0.00	9.11, 0.00	13.14, 0.00
Edge attack F(4,150), p > F	127.96, 0.00	128.05, 0.00	8.34, 0.00	47.72, 0.00	80.24, 0.00	13.65, 0.00
Trial category × edge attack F(8,150), p > F	0.23, 0.99	0.22, 0.99	0.23, 0.99	0.30, 0.97	0.44, 0.90	0.55, 0.82

Table 2

Elastic net classification results summary.

	CG *vs.* CNG	**CNG *vs.* ING**	**CG *vs.* ING**
Accuracy	0.77	0.91	0.77
AUC	0.87	0.91	0.77
AUC p-value	<0.01	=0.01	<0.03